Integration of upward GPR and water content reflectometry to monitor snow properties

(Article begins on next page)

31 August 2024

Integration of upward-GPR and Water Content Reflectometry to monitor snow properties

Authors:

A.Godio, B.Frigo, B.Chiaia - Politecnico di Torino (Italy)

M.Maggioni, M.Freppaz (Università di Torino - Italy)

E. Ceaglio, P. Dellavedova (Fondazione Montagna Sicura - Italy)

Corresponding Author:

Alberto Godio DIATI - Politecnico di Torino

alberto.godio@polito.it

Abstract

We adopt upward Ground Penetrating Radar (up-GPR) and Water Content Reflectometry (WCR) sensors to monitor the seasonal behavior of snow density. Up-GPR permitted to observe at a single fixed station the time lapse response of the electromagnetic signal at the main frequency of 1500 MHz, with the antenna radiating upward from the soil toward the snow surface. Measurements have been performed in a test site on Italian Alps (at elevation of about 2100 m a.s.l.) during the winter season 2014-15 at interval of 30 min. The data processing of radar data involved the traveltime picking and the conversion into snow depth and density. WCR measurements have been useful in order to calibrate the radar response and to retrieve information on the presence of liquid water content.

23 The integration of up-GPR and WCR technology allow us to infer snow high and

24 layering, snow density changes during the winter season and a preliminary

25 estimate of the liquid water content (LWC). For snow in dry condition, we are able to

26 estimate density values through mixing-rules or polynomial formula. Snow density varies during

27 the season in a range between 250-450 kg/m^3; the results are in good agreement with the results of

28 the ground-truth. For snow in wet condition, the residuals of the electrical permittivity, after a trend

29 removal on the original WCR data permitted to estimate a liquid water content in the range between

30 3-5 %, during some periods of the winter season, according to warmer climate condition.

31 Snow layering and densification processes are monitored by the response of up-GPR: fast

32 phenomena such as wetting front infiltration can be also pointed out even if they appear challenging

33 if other observation are not available (e.g. monitoring with WCR).

Key-words:

Ground Penetrating Radar, Water Content Reflectometry, Snow density, Snow water content

Introduction

The development of non-invasive methods to monitor the density and water content by means of electromagnetic devices is of great interest, because of their capability to operate in complex logistical condition (slopes, remote areas, extreme weather condition,...). Moreover, the detection and monitoring of the mechanical properties, jointly with the liquid water content, are relevant in the analysis of snow-gliding phenomena. Glide-snow avalanches occur when the entire snowpack glides over the ground until an avalanche releases. Snow gliding processes and glide-snow avalanches are mainly caused when a reduction in friction at the base of the snow cover occur (e.g. Schweizer et al. 2003); this phenomena is related to an increase of liquid water.

Measurement techniques for the liquid water content of snow are well developed and based on the electromagnetic properties, such as Time-domain Reflectometry, Water Content Reflectometry and Ground Penetrating Radar (Koh et al., 1996). Other methods require an open snow pit and thus are destructive.

The electromagnetic properties of snow are relevant because of their sensitivity to density (e.g. Godio and Rege, 2015a, Godio, 2016) and liquid water content (LWC) changes. Moreover, water percolation in snow or the presence of a wet basal layer in the snow cover are potentially (e.g. Godio and Rege, 2015)

57 associated to the triggering of avalanche and local instability phenomena.

58 Time-domain reflectometry (TDR) allows for non-invasive continuous monitoring of

59 snow properties within the snowpack (e.g. Schneebeli and others, 1998). Water

60 Content Reflectometry (WCR) is based on similar technology of TDR (e.g. Stein,

61 1997) and can be easily adapted for automatic monitoring of electromagnetic

62 properties of snow (e.g. Godio et al. 2015b).

63 Ground Penetrating Radar (GPR) is a promising technology for many applications

64 in snow science, and quantitative results on snow stratigraphy based on radar

65 signals referring on the temporal evolution at a specific site, are of great

66 interest in risk avalanche prediction. Ground Penetrating Radar (GPR) is widely

67 adopted to detect the snow depth and snow-water equivalent (e.g. Godio, 2008,

68 Rege and Godio, 2012, Previati et al. 2011, Forte et al. 2013). The method

69 provides an accurate estimate of the snow depth with much less time spent in the

70 field compared to conventional measurements (e.g. Godio and Rege, 2016, Bruland

71 et al., 2000). Pulsed and frequency modulated GPRs are promising methods, even

72 if they require great care in data processing and calibration as the snow depth

73 is estimated from the traveltime of the radar signal. GPR survey is suitable to

74 cover large areas in an accurate and fast way (e.g. Marchand and al. 2001).

75 The upward Ground Penetrating Radar (up-GPR) is herein adopted to monitor in

76 time lapse modality the snow properties using a single antenna, disposed on the

77 soil and radiating upward (on the snowpack). Up-ward looking GPR is not a

78 novelty in snow monitoring (e.g. Heilig et al, 2009, 2010, Schmid et al., 2014),

79 while TDR and WCR are widely adopted for soil moisture and they can be

80 successfully adopted to estimate and monitor electrical permittivity of snow

81 (e.g. Previati et al. 2011). Otherwise, the integration of GPR and WCR allows us

82 to monitor the time-lapse behavior of snowpack during the winter season by an

83 integrated approach, where WCR data are useful to calibrate the GPR response.

84 We have installed upward-looking GPR with the objective of continuously

85 monitoring the temporal evolution of the seasonal alpine snowpack and deriving

86 snow stratigraphy information from the radar signals. The radar response is here

87 analyzed according to the analysis of the WCR data. Particularly, we focus on

88 determining the snow height, the amount of new snow, snow settlements and liquid

89 water content.

90

91 Materials and Methods

92 The monitoring of snow properties was performed at the flat-field test site of

93 Sant'Anna, located above Gressoney at 2100 m a.s.l. in the Monte Rosa sky resort

94 area. The area is on the foothill of the glaciers of MonteRosa massif in the

95 Western Italian Alps.

96 The equipment has been installed in the test site in September, in order to have

97 enough time to calibrate all the devices before the beginning of the winter

98 season (Figure 1).

99 Particularly the test site was addressed with one up-Ward GPR, with an antenna

100 working at the main frequency of 1500 MHz; the antenna was buried within the

101 soil (see the paragraph on GPR) and the radar cable was protected and sealed

102 within a corrugated pipe in order to avoid damages due to snow load and possible

103 interferences due to liquid water. The radar unit was installed within a plastic

104 box (together with an external battery), and fixed on a vertical rod, inserted

105 into the ground. The power supply for GPR and other electronic devices

106 (datalogger, WCR units, sensors) was guaranteed by two buffer batteries connected to an

107 inverter and powered by a photovoltaic panel

108 Three WCR probes for estimating (locally) the dielectric permittivity of ground and snow were

109 connected to a datalogger unit by means of coaxial cables (protected by corrugate pipe). One probe

110 was installed directly into the ground; two probes were located at different elevation with respect to

111 the ground level in order to detect the properties of the snow. The datalogger unit was located in the

112 same plastic box of the GPR unit and powered by the inverter-photovoltaic power system.

113 Moreover, the test site was equipped with sensors to record meteorological and

114 snow-cover properties; we have installed snow height sensors (HS), an

115 ultrasonic gauges and air temperature, and snow temperature. The HS sensors are

116 based on ultrasonic devices which measure the traveltime of an high frequency

117 pulse, as described in a following paragraph. The sensors were located at an

118 elevation of about 2.5 meters above the ground, as depicted in pictures of

119 Figure 2.

120 The WCR and GPR measurements were performed in the winter season 2014-15.

121 Particularly, the data acquisition refers to the period starting from November

122 to April, with some lack in data because of some malfunctioning of the GPR

123 equipment.

124 Conventional manual snow profiles according to the methodology suggested by

125 Fierz and others (2009) were conducted on a bi-weekly basis close to the test

126 site. Snow density was determined by taking samples of volume of 100 cm^3 at

127 different depth in a snow pit and weighting them on an electronic scale. For

128 each layer recorded in the snow pit, at least two density samples were taken and

129 averaged (Table 1).

130

131 *Electromagnetic properties of snow*

132 The snow is considered as a continuous mixture in which the ice and vapor

133 constituents are themselves treated as individual but interacting continua. Snow

134 on the ground is viewed as an un-saturated three-phase granular material

135 comprised of small grains of ice with interstitial pores partially filled by a

136 single vapor. A small fraction (less than 10 % in volume) of porous voids can be

137 filled by liquid water (wet snow). Bradford et al. (2009) provided an overview

138 on the effect of liquid water content on the electrical permittivity of snow;

139 Lundberg and Thunehed (2000) considered the effect of liquid water on the radar

140 signal into the snowpack. Otherwise, the electrical permittivity of dry snow and

141 ice at different temperature and density has been widely reported (e.g. Evans,

142 1965, Glen and Paren, 1975). In such condition (dry snow), the electromagnetic

143 measurements can be easily and accurately converted into snow density.

144 Particularly GPR survey is suitable to detect snow depth and dielectric

145 permittivity with high resolution, until a depth of several meters (e.g.

146 Previati et al., 2011).

147 Mixing rules or adapted mixtures rules relate the dielectric permittivity of the

148 mixture with permittivity and fraction of volume of each single phase. For dry

149 snow (two-phases), several relationships between the electrical permittivity and

150 snow density are well established (e.g. Looyenga, 1965), while for wet snow,

151 where a small fraction of liquid water provides a marked increase of electrical

152 permittivity of the mixtures, the relationships are more challenging, because of

153 the complexity to distinguish between the effect of changes of snow density from

154 liquid content on the observed dielectric permittivity.

155 The radar performances in terms of reflectivity, vertical resolution and

156 penetration depth have been widely discussed in literature (e.g. Godio, 2007,

157 2009, Previati et al., 2011). From an electrical point of view, the dry-snow can

158 be considered as non-conducting medium; the electromagnetic wave does not suffer

159 of the intrinsic attenuation as it propagates through the snowpack and it can be

160 assimilated to a lossless medium, in such a case, the complex permittivity is

161 equal to the real permittivity. For instance a granular snow at high density

162 (>600 kg m^{-3}) is characterized by a wavelength of 0.2 m (at 1 GHz) and a

163 theoretical vertical resolution of 0.05 m (assuming the vertical resolution

164 equal to 1/4 of the wavelength).

165 At the interface between two snow layers or between the snowpack and the air,

166 considering a normal plane wave incidence, the reflection (Γ) and transmission

167 coefficient (τ) are:

168

169 $$\Gamma = \frac{\eta_2 - \eta_1}{\eta_2 + \eta_1}$$

170

171 $$\tau = \frac{2\eta_2}{\eta_2 + \eta_1}$$

172

173 where η is the intrinsic impedance (Ohm m) of layers 1 and 2.

174 When a signal meets a thin snow layer, multiple reflections between the two

175 interfaces limiting this layer could arise. The amplitude of the resulting wave

176 is dependent on the interferences between the reflected waves, which can be

177 constructive or destructive in function of the traveltime into the layer, itself

178 dependant on the thickness and the snow density.

179 If both geometric and intrinsic attenuations can be neglected, and if the signal

180 is a continuous plane sinusoid, the resulting reflection coefficient ranges

181 between 0 for purely destructive interferences to one or more maxima, for

182 constructive interferences. Considering a thin snow layer (medium 2), embedded

183 into a medium 1, and assuming a thickness *(t)* of the layer comparable to the

184 wavelength in the first medium, an appropriate expression for the reflection

185 coefficient is (Godio, 2009):

186 $$\Gamma = \frac{\Gamma_{12}(1 - e^{i\beta})}{(1 - \Gamma_{12}^2 e^{i\beta})}$$

187 where

188 $$\beta = \frac{4\pi t}{\lambda_1}$$

189 and λ_1 is the wavelength in the snow layer 1. As the wavelength of the signal is

190 related to the wave velocity, it depends on the density of the snow pack, and

191 therefore the reflection coefficient is affected by the density variation.

192 A detailed description of the relationship between thickness of a thin snow

193 layer and the reflection coefficient at different frequencies is reported in

194 Godio (2009). For a thin high density snow layer ($\varepsilon = 3$) embedded in a softer

195 snow, with a permittivity value equal $\varepsilon = 2$, the trend of reflection coefficient

196 with respect to the frequency is dependent by the thickness of the layer.

197 In the frequency range from 100 MHz up to 2 GHz, the trend can be assumed linear

198 for very thin layers (t = 5-10 mm). For increasing thickness (e.g. 50-100 mm),

199 the reflection coefficient assumes a sinusoidal behavior with peaks at different

200 frequencies. For instance, a thin layer of 50 mm is characterized by a maximum

201 of reflection coefficient is at 1 GHz. For a thickness of 100 mm, at the

202 reference frequency of 1 GHz, the reflection coefficient is almost null.

203 As far as the amplitude of the reflection coefficient is concerned, at the

204 frequency of 1 GHz, the values vary from 0.25 for a thin layer of 5 mm, to 0.05

205 for the layer of 10 mm and to 0.2 for the layer of 50 mm.

206

207 *Dry snow*

208 For dry snow, a simple relationships between the snow density and the

209 electromagnetic properties yields. The Robin's equation, for instance, is an

210 empirical relationship between density and electrical permittivity (ε) (Kovacs

211 et al. 1995):

212 $$\varepsilon=(1+0.845\cdot\rho)^2 \qquad\qquad [1]$$

213 where ρ is the specific gravity of firn and ice (with respect to pure ice) and

214 electrical permittivity is the relative value with respect to vacuum

215 (dimensionless).

216 The technical literature report many variants of mixing models to relate the snow density and

217 dielectric permittivity. The Robin's equation is a simple polynomial fitting of the straightforward

218 Looyenga (1965) formula, which has been widely used for a bi-phasic mixture of snow. A

219 comparison of the validity and drawbacks of different mixing rule is out of the scope of the

220   manuscript, a detailed description of different approaches is well developed in Booth et alii (2013).

221   We just infer a range of density values, according to the limits of accuracy of the adopted method

222   (Looyenga, 1965).

223   In terms of wave velocity (v) the following relationship yields:

224     $v = c/(1 + 0.845 \cdot \rho)$ [m/ns]   [2]

225   where c is the wave velocity in vacuum (here in m/ns). In the velocity range of 0.2 m/ns to 0.24

226   m/ns the specific gravity almost double (from 0.3 to 0.6).

227   The relationship between the radar traveltime (twt) and the specific gravity becomes:

228     $twt = 2d/c \cdot (1 + 0.845 \cdot \rho)$ [ns]   [3]

229   where d is the snow depth; finally we estimate the Snow Water Equivalent (SWE) as:

230     $SWE = \rho_{ice}/2 \cdot 0.845 \cdot (c - v) \cdot twt$ [kg/m^3 m]   [4]

231

Wet snow

233   Relationships between the electromagnetic parameters and snow properties are

234   usually based on mixing rules, where the bulk electrical permittivity depends on

235   the fraction volume of each single phase: ice as solid phase, gas and free water

236   (e.g. Sihvola,et al. 1985). A polynomial relationship (Denoth, 1994) between

237   electrical permittivity, density and water content is here adopted:

238     $\varepsilon_{snow} = 1 + 1.92\ \rho_{snow} + 0.44\ \rho_{snow}^2 + 0.187\ \theta_w + 0.0045\ \theta_w^2$ [5

239   ]

240   where ε_s is the dielectric permittivity of the snow, ρ_{snow} (g/cm^3) and θ_w (%) are density and water

241   content, respectively. For dry-snow (neglecting the water content), the equation [5] is similar to

242   standard formulation, usually adopted to estimate density values of dry snow (Godio, 2009, Godio

243   and Rege, 2015a). The sensitivity of the electrical permittivity to the water

244 content effect is demonstrated by analysing the behaviour of the formula [5].

245 An increase of 3-5 % of liquid content provides a relative increase of the

246 electrical permittivity of more than 20-35 %, as discussed in other papers (e.g.

247 Godio, 2016).

248 When the the water content is negligible in the reference period, we convert the

249 WCR response in density values using formula [1].

250

WCR data acquisition

252 Water Content Reflectometer (WCR) measurements are based on a radio-frequency

253 signal (some decades of MHz) traveling along a two/three rod's probes, acting

254 as a transmission lines, and observing the period of the reflected signal.

255 Particularly, our device consists in an electronic circuit embedded in the probe

256 of two stainless steel rods, 30 cm length, connected to a datalogger. The signal

257 velocity is related to the electromagnetic properties of the embedded material;

258 the electrical permittivity of the material is computed from the observed

259 period.

260 Two WCR sensors were located at elevation + 70 cm (WCR 2) and + 40 cm (WCR 3)

261 above the ground; a third sensor was located 5 cm below the surface to monitor

262 the interaction between the snow pack and soil.

263

Laboratory calibration of WCR

265 We measured the WCR's output in air and de-ionized water at different

266 temperatures,   to check the temperature dependence of the electrical

267 permittivity water (Hamelin et al., 1998). The tests were performed in a

268 climatic chamber by monitoring the temperature of the water sample with a

269 thermometer model Fluke S4 I. The frequency-dependence of the constituents of

270 the air and ice is herein neglected as Kelleners et al. (2005) suggested; this

271 is admitted in the bandwidth of approximately 175 MHz of the functioning of the

272 adopted sensor.

273 A correction of the observed WCR period accounts for the temperature effect of

274 water, ice and air components. A polynomial of 2nd degree is used to correct the

275 observed data in the range between 0 and −8 ° C. By considering these effects,

276 the electrical permittivity of water decreases gradually during the freezing

277 phase; at −12 ° C, the (relative) electrical permittivity assumes values close

278 to 3.2; by increasing the temperature, the permittivity slowly decreases up to

279 values of about 3 (at 0 ° C), when the melting is starting. Those values agree

280 with literature data on the electromagnetic response of water below 0 ° C.

281

282 *GPR data acquisition*

283 The upward Ground Penetrating Radar (up-GPR) is a pulse-type radar with an

284 antenna, at the main frequency of about 1500 MHz, posed on the ground surface

285 and radiating upward on the snow.

286 The basic principle is the same of the conventional GPR adopted from the

287 surface; we use a transmitter antenna and a receiver one in bi-static

288 configuration with offset of few cm. The antennas were buried into the ground at

289 the beginning of the winter season, and they have been disposed in such a way

290 that the radiation of the electromagnetic energy was oriented from the ground

291 up-ward. During the wintertime, the ground and the antenna were covered by the

292 snow pack; therefore, the radiation energy propagates from the ground into the

293 snow.

294 A good compromise between resolution and signal quality and penetration depth,

295 is achieved by using (commercial) antennas in the frequency range between 1 - 2

296 GHz. This range is suitable to operate with good performance up to a snow

297 thickness of about 2-3 meters that has not been reached during the monitored

298 season. In environments with very huge snow accumulation (more than 3 m), the

299 adoption of commercial antennas with lower main frequency, such as 900 MHz, is

300 suggested and offers good performance (e.g. Previati et al. 2011). Snow humidity

301 (moisture content) does not seem an obstacle (at least in that site) because we

302 estimate that a maximum value of less than 10 % in volume of liquid water is

303 filling the pore volume during the melting period. This quantity does not affect

304 the signal quality.

305 Snow temperature affect the accuracy of evaluating dielectric permittivity,

306 because of the dependence of dielectric to temperature below 0° Celsius.

307 This must be considered in further research activity.

308 The system sends a series of pulses every 30 min to get the A-scans and all the

309 traces are gathered to obtain a B-scan, where along the x-axis we indicate the

310 reference time instead of a distance, as in standard acquisition. Because the

311 low attenuation of the electromagnetic waves in the snow, high frequency can be

312 adopted; the installed system operates at the main frequency of 1500 MHz, with a

313 frequency band of approximately 1 GHz.

314 We extend the monitoring period from November 2014 till April 2015; measurements

315 were performed every 30 min, with a stacking of 256 traces, on a window time of

316 50 ns and 1024 sampling for each traces. An analog-to-digital converter of 16

317 bit was adopted. Results were stored in separated files in the internal memory;

318 and then downloaded for subsequent data processing, because of the complexity of

319 handling an effective remote control of the system.

320

321 *Data processing*

322 The flow chart of the integrated data processing of GPR, WCR and other data is

323 depicted in figure 3. Particularly, the standard data processing of B-scan

324 involves the edit and removal of distortions of the main-bang, filtering of low

325 frequency electronic noise with dewow, applying the background removal to

326 minimize the main bang effect and reduce coherent "horizontal" noise, The

327 background removal has been performed by averaging 5 traces and subtract the

328 results from the B-scan.

329 We applied a the gain recover procedure to remove the acquisition gain, to

330 apply a divergence compensation, We didn't introduce the correction for the

331 intrinsic attenuation because of the negligible dissipation effect of

332 electromagnetic energy in the snow (low attenuation coefficient). The band-pass

333 filter removes the unwanted energy out the frequency band of 1000 - 2200 MHz;

334 finally a trace stacking was performed to get a single traces every two hours.

335 (stacking of four A-scan).

336

Snow surface picking

We adopt a semi-automatic method, which requires manual interaction according to the following steps:

- a phase follower algorithm detects the peak of the same half-cycle, following the signals at the equal phase;

- If two consecutive traces deviated, we checked whether the height of the snow surface changed due to accumulation, settling or melt; this step is performed by comparing the GPR data with the high of snow (HS) given by ultrasonic measurements (in the period of overlap of the two measurements); an rough evaluation on settling and melting phase has been possible thanks to the analysis of temperature data;

- If none of these changes appeared in the recorded weather data, and deviations in the phase sequence occurred (e.g. while surface crusts were persistent or surface melt happened), we neglected phase reversals;

- During strong accumulation and melt events, manual picking is necessary to reset the follower to the correct phase.

Finally, internal layers were picked in a similar way to the procedure of the semi-automated snow surface picking algorithm.

New snow height (NSH)

Ultrasonic sensors are conventional instrument for measuring snow height; they

358 are able to measure the distance to the snow from the surface.

359 Particularly, the ultrasonic level sensors work by the "time of flight"

360 principle (basically like the GPR…) using the speed of sound. The sensor emits

361 a high-frequency pulse, generally in the 20 kHz to 200 kHz range, and then

362 observes the echo at the snow-air interface. The pulse is transmitted in a cone,

363 usually about 6° at the apex. The pulse is reflected at the level surface

364 (snow) back to the sensor, now acting as a receiver and then to the transmitter

365 for signal processing. A correction of the speed of sound because of the

366 temperature is necessary for an accurate estimate of the distance between the

367 transmitter-receiver sensors and the snow surface. Usually an accuracy of about

368 2 % is obtained. Data have been acquired every 30 minutes, and recorded in a

369 data logger. A sketch of the installation of the sensors is reported in figure

370 1.

371 During a snowfall, snow height increases and the load of the new snow provides

372 for the settlement of the underlying layers. In such a case the new snow height

373 is always underestimated, i.e. the amount of new snow cannot be measured

374 automatically.

375 The radar, however, still records the reflection of the old snow surface after

376 it was covered by new snow. Therefore by subtracting the two-way travel time of

377 the reflection of the old snow surface from the time of the new snow surface, a

378 more accurate estimation of the fresh snow height can be performed.

379 The process requires an assumption of the fresh snow density. At the elevation

380 of the test site (above 2 100 m a.s.l.), the density of the new snow is usually

381 in the range of 50–100 kg/m^3. The wave velocity is in the range between 0.263 –

382 0.274 m/ns; we calculated the new snow height (NSH) using the following

383 equation:

384 $\qquad NSH = (Twt_1 - Twt_0)*c / 2 (1+0.845 \rho)$

385 where c is the wave velocity in vacuum and ρ is the specific gravity of snow

386 with respect of pure ice (assumed equal to 920 kg/m^3), and Twt_1, and Twt_0 are the

387 traveltimes of the "new" reflection and "old" reflection, respectively.

388 The accuracy in the detection of the NSH depends on the uncertainty in the

389 assumption of snow density and on the accuracy in the picking of the traveltime

390 differences. A conservative estimate assumes the uncertainty in the estimate of

391 traveltime about 0.05 ns. Therefore, the accuracy in the new snow estimate is

392 computed according to the following analysis:

393 $\qquad \Delta NHS = |\partial NHS/\partial twt|\cdot\Delta twt+ |\partial NHS/\partial \rho|\cdot\Delta\rho$

394 $\qquad \Delta NHS = c/2 (1 + 0.845 \rho) \Delta twt + (0.845 c\, dt)/(2 (1+ 0.845 \rho)^2) \Delta\rho$

395 where dt = Twt1 - Twt0, and if the upper and lower boundary are considered:

396 $\qquad NHS^+ = (dt+\Delta t) *c / (2 (1+0.845 (\rho-\Delta\rho))$

397 $\qquad NHS^- = (dt-\Delta t) *c / (2 (1+0.845 (\rho+\Delta\rho))$

398 For a gravity value of 0.13 with an uncertainty of 0.025, and assuming a

399 differences of traveltimes of 5 ns, and a interval of 0.5 ns, the fresh snow

400 height results:

401 $\qquad NHS= 0.68+/-0.08$ [m]

402 with a relative uncertainty of about 12 %.

403

Processing of WCR data

The densification process is a long term process that could provide gradual variation of the response in time during the season. Therefore abrupt changes (in time) of the WCR response are mainly related to the effect on the dielectric permittivity of the liquid water content in the snow. Particularly, time series of WCR data are processed by separating the short term oscillations of electrical permittivity from the long term ones, adopting a de-trend analysis, as depicted in figure 4. Finally the water content is estimated from the residual data of the electrical permittivity, through formula [5].

Results and Discussion

WCR data

The seasonal response of WCR data is shown in figure 4. WCR 1 refers to the response of the probe into the soil. WCR2 and WCR3 are the probe at elevation of +40 cm and 70 cm above the ground (on the snow); the data processing of observed electromagnetic response involves two steps: i) the analysis of the time series, ii) the conversion of the electrical permittivity into snow density and liquid water content by applying mixing rules.

We stress the relevancy of monitoring the ground condition, by observing the water content in the uppermost surface soil. We observed all along the season the presence of high water content (almost close to the saturation) and no frozen phenomenon of the soil: this is of interest both for modeling the

426 thermal regime of the snowpack, and for linking different sliding condition of

427 the snowpack at the interface with the ground.

428 The high frequency oscillations at small amplitude are related to the influence

429 of the diurnal temperature, because the measurements are not compensated by the

430 temperature correction; the effect is more pronounced on the WCR 2 that is

431 closer to the snow-air interface, where the exposure and influence of solar

432 radiation and air temperature is more relevant.

433 Moreover the trend of the data of WCR 2 indicates a marked increase of the

434 electrical permittivity of the uppermost layer of the snow pack; the observed

435 values are similar to the values assumed for ice. In this case, like for the

436 seasonal data, we can't distinguish if the effect on the electrical

437 permittivity is caused by densification processes or because a increase of free

438 water content is occurred. The density values have been computed according to

439 the formula [1]; the relationships allowed us to convert the dielectric

440 permittivity of the WCR data into snow density values. Particularly, we observe

441 how the uppermost layers are characterized all over the season by density in the

442 range between 250-300 kg/m^3, while at deeper level, density values are around

443 400-450 kg/m^3. Those ranges are in good agreement with the values observed on

444 samples collected at different time in snow-pits (Table 1). For the density

445 range in those ranges, the wave velocity is between 0.22-0.24 m/ns.

446 Figure 5 shows a detail of the electrical permittivity response, observed at

447 sensor WCR2, and the de-trend analysis herein adopted in order to separate

448 short-term and long-term oscillations. The residual are used to estimate the

449 liquid content within the snow pack, according to the procedure aforementioned.

450

GPR data

452 A general overview of the up-GPR response is depicted din figure 6. We plot the GPR data

453 collected in the period January to April 2015. Unfortunately because of a malfunction of the GPR

454 system some data are missing in February. A qualitative comparison between the GPR data and the

455 measures of snow height collected with the ultrasonic device show a good agreement between the

456 two data sets in terms of estimate of snow accumulation at the ground.

457 GPR image (figure 7) shows the temporal evolution of the snow depth accumulated at soil; an

458 average value of 0.23 m/ns is adopted to convert the traveltimes in to snow elevation on the ground.

459 This value has been computed according to an estimate of the average dielectric permittivity

460 derived from the WCR data; particularly we have observed an average value all over the season of

461 about 1.6 -/+ 0.1 (1 Standard Deviation) for the probe WCR 2 and 1.8 -/+ 0.1 (1 Standard

462 Deviation) foe WCR 3. This yields to an average estimate of the dielectric permittivity of the snow

463 pack of 1.7 -/+ 0.2; the wave velocity is therefore in the range of 2.2 m/ns and 2.4 m/ns, or 0.23-

464 /+0.1 m/ns. The adopted velocity value correspond to an average density of 350 kg/m^3; this value is

465 consistent with the range of values observed all over the season with locally measurements of snow

466 in snow pit (Table 1).

467 The radar section shows several phenomena, that have been highlighted with caps letters.

468 Particularly letter A refers to an abrupt decrease of the snow height just after the first snowfall in

469 November. This is caused by a marked increase in the average temperature in that period,

470 responsible both for a rapid snow settlement (compaction), both causing the formation of a basal ice

471 crust (letter B) and probably also a rapid melting of the snow pack occurred. Subsequent snow falls

472 (letter C and D) provided for an abrupt increase of the snow height in the day from 9 to 11

473 December. Other snow fall events are pointed out with letter E,F.

474 A sharp increase of reflectivity of the inner features within the snow pack are highlighted with

475 letters B, G and H. Feature B refers to the formation of a basal crust, subsequent to the partial melt

476 and re-frozen of the snow pack at the beginning of December; features G and H are instead located

477 in the uppermost zone of the snow pack, close to air-snow interface. Two different explanations can

478 be given: i) an increase of the humidity of the new snow with respect to the old one provide an

479 increase of the contrast of the electromagnetic properties between new and old snow; ii) the new

480 snow is characterized by very low density, with respect to the older one; this provides an high

481 reflection coefficient between new and old snow but with a reverse sign with respect to the case i).

482 A detailed analysis of the phase behavior could be helpful in better understating the reason of the

483 hot spots of reflectivity is still in progress.

484 We also observe a gradual decrease of the snow depth after the main snowfalls,

485 according to snow settlement because of the thermal or mechanical densification

486 processes. This is well depicted in figure 7 by analyzing the trend of the air-

487 snow interface, for instance in between event E and F and between F and G.

488 We note well separated reflection events into the snowpack; the snow layers that

489 are detectable in the radar image refer to layers with different density values

490 within the snow pack. We can outline the event in between features G and H;

491 pointed out with a dashed black line. This event refers to a reflection of a

492 layers into the snowpack, that shows a gently decrease of the snow-high with

493 time. .

494 Above the snow-air reflection some weaker artifacts can be observed (letter M in figure 7); those

495 artifacts are associated to multiple reflections of the main features (layers) within the snow pack.

496 This is consistent with the similarity of the trend of the artifacts (multiples) and the inner reflectors.

497 The high contrast of dielectric permittivity between the snow pack and the air (2.5 snow, 1 air)

498 explain how some energy can be trapped within the uppermost snow layers, generating the multiple

499 response.

The analysis of the behavior at the end of the season (Figure 8) reveals the relationship of radar signal with the gradual snow melting; particularly, this effect started at the beginning of April and can be observed till the end of April. We note the similar high frequency (daily) fluctuations of the radar signal at snow-air interface, that can be also observed in the snow depth (ultrasonic data). This corroborates the assumption of the relationship between the oscillations of the signals and the partial frozen-and melting phase of water within the snow pack. This phenomena provides for slight but detectable (according to the instrumental accuracy) behavior of the expansion and contraction of the snow pack because of different density of the snow pack during the partial-melting phase and during the re-frozen period. The fluctuations are related to the different densities of the two phases of water.

Our experiment setup is different from that addressed in similar research activity. For instance Schmid et al. (2015) proposed an interesting combination of up-GPR and Global Positioning System devices to monitor snowpack properties. In particular they installed up-GPRand a low-cost GPS system below the snow cover and observed the evolution during two winter seasons. Applying external snow height (HS) information, they demonstrated as both methods provided consistent liquid water content estimates in snow, based on independent measurements of travel time and attenuation of electromagnetic waves. We obtained similar results by integrating up-GPR with WCR information, even if we focus on density evaluation more then on LWC. Moreover, we focus on the behavior of the ground just below the snow cover and we demonstrate (in this case) that the soil has been, during all the winter season in not frozen condition. This has relevant implication for the analysis of water exchange between the ground and the snow pack and also in the evaluation of thermal regime at the snow-ground interface.

Snow depth and temperature

The analysis of snow depth trend from January to April points out the several precipitation events mostly occurred in March (Figure 9). The climate conditions of the site have been responsible of relevant snow falls, followed by abrupt and marked snow settlements We highlight note the event of February, the 5-6th: an accumulation of about a 40 cm of new snow occurred but the day after an abrupt increase of the air temperature provided for a sudden snow settlement (more than 30 cm). This was followed by a few days of stability, with a small reduction of the snow depth (few cm), according to the decrease of the air temperature. This fast snow settlement is also visible in several events in February and March.

The snow settlement appears very sensitive to the diurnal fluctuations of the air temperature, and obviously to the general climate conditions. The response is very fast, with relevant consequence to the probability of an increase of free water content in the uppermost layers of the snow. This could be analysed in detail considering the reflectivity and phase of the radar signal, for instance.

The snow depth reached a maximum values of about 120 cm and then gradually decreased till less than 60 cm at the end of April. Small fluctuations of snow depth can be observed with a daily frequency. We associate this effect to the melting and refrozen of ice-water in the pore space of the snow, that slightly modifies the snow depth.

The snow melting started approximately at the beginning of April; the comparison

547 between the snow depth, collected by ultrasonic measurements, and the air

548 temperature shows the correlation between the average temperature and the snow

549 melting phase. After a last relevant snow fall, occurred during the days April,

550 5-6th, the average temperature raised up to values above 0° Celsius , with

551 diurnal fluctuations between -5 and + 10 Celsius degree.

552

553 *Soil water content*

554 The response of WCR in the soil shows a regular and almost constant trend all

555 over the monitoring period. Some small fluctuations could be of interest mostly

556 because they appear well related to the fluctuations observed in the data of

557 WCRs located in the snow (e.g. the event at middle of January).

558 We note that the values of about 45-55 % of water content are compatible with

559 the nature of the uppermost part of the soil, characterised by a soil with high

560 porosity and low permeability. Therefore a high water content is observed and

561 the soil remains in almost saturated condition for long time. The early snow

562 falls at the end of November provided for a enough thickness of snow cover to

563 avoid the water within the soil to freeze. This condition of unfrozen soil

564 remains for all the winter season.

565

566 ## Final remarks

567 We have proven that the integration of WCR and GPR response is an effective tool

568 to monitor the seasonal variation of snow properties. For snow in dry condition,

569 we are able to estimate density values through mixing-rules or polynomial

570 formula. The water content is estimated by performing the analysis of the

571 residuals of the electrical permittivity, after a trend removal on the original

572 WCR data.

573 Snow layering within the snow pack, and densification processes are monitored by

574 upward-GPR: fast phenomena such as wetting front infiltration are of relevant

575 interest but they are challenging if evidences coming from other observation are

576 not available (e.g. monitoring with WCR). Even if an accurate analysis of

577 volumetric water content within the snowpack appears still challenging, we will

578 work on the spatial variability. This will require the development of low cost

579 (simplified, e.g. multiplexing devices) radar system must be developed to drive

580 an array of antennas. WCR is (rather) low-cost devices that can be routinely

581 integrated in snow-weathering stations.

582 The integration of WCR and up- GPR offers a good accuracy in monitoring the

583 average values of snow density. Moreover upward GPR, WCR probes and conventional

584 snow depth observations permit detailed analysis of snow deposition, the

585 settlement phase, densification process and melting and frozen phase.

586 The further data processing would focus on the analysis of the observed data

587 with marked variations of snow depth and with an increase of free water within

588 the pore volume of the snow pack. These phenomena, jointly with the analysis of

589 the temperature trend, could be associated to the probability of the occurrence

590 of snow gliding.

591

592 **Acknowledgements**

595

596 **Table 1:** snow depth and density at two different elevation above the ground
597 during the winter 2014-15, observed in pits.
598

Date	17-Dec	21 - Dec	31 - Dec	7 - Jan	28 - Jan	4 - Feb	12 - Feb	18 - Feb	4 - Mar	11 - Mar
Snow Depth [cm]	80	70	65	64	87	99	110	125	132	113
Density at elevation + 0.7 m [kg/m^3]	120-340	200	-	-	200	260	270	300	320	400-340
Density at elevation + 0.4 m [kg/m^3]	340-420	300-360	320	400	400	400	270	380	400	400

599

References

Booth A. D., Mercer A., Clark R., Murray T., Jansson P., Axtell C., 2013. A comparison of seismic and radar methods to establish the thickness and density of glacier snow cover. *Annals of Glaciology* 54 (64) , 73–82, doi:10.3189/2013aog64a044

Bradford J.H., Harper J.T. and Brown J., 2009. Complex dielectric permittivity measurements from ground-penetrating radar data to estimate snow liquid water content in the pendular regime. *Water Resour. Res.* , 45 (8), W08403 (doi: 10.1029/2008WR007341)

Bruland O., Sand K., Killingtveit A., 2000. Snow distribution at a high Arctic site at Svalbard. *Nordic Hydrology* 32:, 1–12.

Denoth, A., 1994. An electronic device for long-term snow wetness registration. *Annales of Glaciology*, 19, 104–106.

Evans S. 1965. Dielectric properties of ice and snow. *Journal of Glaciology* 5: 773–792.

Glen J.W, Paren J.G., 1975. The electrical properties of snow and ice. *Journal of Glaciology* 15, 15–38.

Fierz, C., Armstrong, R.L., Durand, Y., Etchevers, P., Greene, E., McClung, D.M., Nishimura, K., Satyawali, P.K. and Sokratov, S.A. 2009. The International Classification for Seasonal Snow on the Ground. IHP-VII Technical Documents in Hydrology N° 83, IACS Contribution N° 1, UNESCO-IHP, Paris.

Forte, E., Dossi, M., Colucci, R.R., Pipan, M., 2013. A new fast methodology to estimate the density of frozen materials by means of common offset GPR data. *Journal of Applied Geophysics*, 99, 135–145.

Forte, E., Pipan, M., Godio, A., Francese R., 2015. An overview of GPR investigation in the Italian Alps. *First Break,* 33, 8, 61–67.

Godio A. 2008. Performance and experimental evidence of GPR in density estimates of snowpack. *Bollettino di Geofisica Teorica e Applicata* 49: 279–298.

Godio A. 2009. Georadar measurements for snow cover density. *American Journal of Applied Sciences* 6 : 414–423.

Godio A., Rege R.B., 2015a. The mechanical properties of snow and ice of an alpine glacier inferred by integrating seismic and GPR methods, *Journal of Applied Geophysics*, 115, 92–99, http://dx.doi.org/10.1016/j.jappgeo.2015.02.017.

Godio A., Franco D., Chiaia B., Frigo B., Dublanc L., Freppaz M., Maggioni M., Ceaglio

E and Dellavedova P. ,2015b. Seasonal Monitoring of Snow Properties by WCR and up-GPR, EAGE Near Surface Geoscience 2015 – 21st European Meeting of Environmental and Engineering Geophysics, Torino

Godio, A., Rege, R.B., 2016 . Analysis of georadar data to estimate the snow depth distribution, *Journal of Applied Geophysics*, 129, 92–100, http://dx.doi.org/10.1016/j.jappgeo.2016.03.036.

Godio, A., 2016. Multi Population Genetic Algorithm to estimate snow properties from GPR data. Journal of Applied Geophysics, 131, 133-144. DOI: 10.1016/j.jappgeo.2016.05.015

Hamelin, J., Mehl, J.B., Moldover, M.R., 1998. The static dielectric constant of liquid water between 275 K and 400 K near the saturated vapor pressure. *International Journal of Thermophysics*, 19, 1359–1380.

Heilig A., Schneebeli M. and Eisen O. 2009. Upward-looking ground-penetrating radar for monitoring snowpack stratigraphy. *Cold Reg. Sci. Technol.*, 59 (2–3), 152–162 (doi: 10.1016/ j.coldregions.2009.07.008)

Heilig A., Eisen O. and Schneebeli M., 2010. Temporal observations of a seasonal snowpack using upward-looking GPR. *Hydrol. Process.* , 24 (22), 3133–3145 (doi: 10.1002/hyp.7749)

Kelleners, T.J., Seyfred, M.S., Blonquist, J.M., Bilskie, J. and Chandler, D.G, 2005. Improved interpretation of water reflectometer measurements in soils. *Soil Sci. Soc. Am. J.* 69, 1684–1690.

Koh G., Yankielun N.E., Baptista A.I., 1996. Snow cover characterization using multiband FMCW radars. *Hydrol. Process.* 10, 1609–1617.

Kovacs A., Gow A.J., Morey R.M., 1995. The in-situ dielectric constant of polar firn revisited, *Cold Region Science and Technology,* 23, 245–256.

Looyenga, H., 1965. Dielectric constant of heterogeneous mixtures. *Physica* , 31, 401–406.

Lundberg A., Thunehed H. Bergstrom J., 2000. Impulse radar snow surveys – influence of snow density. *Nordic Hydrology* , 31, 1–14.

Lundberg A. and Thunehed H., 2000. Snow wetness influence on impulse radar snow surveys: theoretical and laboratory study. *Nord. Hydrol.* , 31 (2), 89–106 (doi:

662 10.2166/nh.2000.007)

663 Marchand W.D., Bruland O, Killingtveit A. 2001. Improved measurements and analysis of
664 spatial snow cover by combining a ground based radar system with a differential global
665 positioning system receiver. *Nordic Hydrology*, 32, 181–194.

666 Previati M., Godio A., Ferraris S., 2011. Validation of spatial variability of snowpack
667 thickness and density obtained with GPR and TDR methods. *Journal of Applied Geophysic*s,
668 75, 284–293, DOI: 10.1016/j.jappgeo.2011.07.007.

669 Rege, R.B., Godio, A., 2012. Multimodal inversion of guided waves in georadar data,
670 *Journal of Applied Geophysics*, 81, 68–75, DOI: 10.1016/j.jappgeo.2011.09.021.

671 Sand K, Bruland O. 1998. Application of georadar for snow cover surveying. *Nordic*
672 *Hydrology* 29 : 361–370.

673 Schmid L., Heilig A., Mitterer, C., Schweizer, J., Maurer, H., Okorn R., Eisen O.,
674 2014. Continuous snowpack monitoring using upward-looking ground-penetrating radar
675 technology. J*ournal of Glaciology*, 60, 221, 2014 doi: 10.3189.

676 Schmid, L., F. Koch, A. Heilig, M. Prasch, O. Eisen, W. Mauser, and J. Schweizer
677 (2015), A novel sensor combination (upGPR-GPS) to continuously and nondestructively
678 derive snow cover properties, *Geophys. Res. Lett.,* 42, 3397-3405,
679 doi:10.1002/2015GL063732.Schneebeli M., Coleou C., Touvier F. and Lesaffre B. 1998.
680 Measurement of density and wetness in snow using time-domain reflectometry. *Ann.*
681 *Glaciol.*, 26 , 69–72

682 Schweizer, J., Jamieson, J.B. and Schneebeli, M, 2003. Snow avalanche formation. *Rev.*
683 *Geophys.*, 41 (4), 1016 (doi: 10.1029/ 2002RG000123)

684 Sihvola, A., Nyfors, E. and Tiuri, M., 1985. Mixing formulae and experimental results
685 for the dielectric constant of snow*. Journal of Glaciology,* 31, 163–170.

686 Stein, J., Laberge, G. and Lèvesque, D. 1997. Monitoring the dry density and the liquid
687 water content of snow using time domain reflectometry. *Cold Regions Science and*
688 *Technology*, 25, 123–136.

689

690

691

Captions

Figure 1: sketch of the test site with position of sensors.

Figure 2: pictures of the test site; a) installation of the equipment; b) winter time at the test site!

Figure 3: flow chart of the data processing and data integration between GPR and WCR.

Figure 4: winter season 2014-2015, seasonal behavior of WCR response, a) WCR 1 refers to soil water content; b) WCR2 and WCR3 are the probe at elevation of +40 cm and 70 cm above the ground (on the snow).

Figure 5: a) example of de-trend analysis to separate the short term effect and the long term behavior of WCR data; the residuals of the dielectrical permittivity (short term behavior) are related to the effect of the liquid water content.

Figure 6: a) up-ward GPR response, period January 2015 - April 2015; blank sectors refer to data missing; b) snow depth by ultrasonic measurements (data missing in the period January-February 2015).

Figure 7: detail of up-ward GPR response in December2014 , letters A refers to an abrupt compaction and or melting of the snow pack; C,D E,F, refer to the radar response to the new snow falls, features B, G,H are hot spot of reflectivity within the snowpack, N indicates artifact because of multiple reflections. (see the text for further explanations).

Figure 8: a) detail of up-ward GPR response during April; the reflection vent of air-snow interface show some pulsation; a similar behavior is depicted by the ultrasonic response (snow height), in figure b).

Figure 9: Air temperature trend and snow depth according to ultrasonic data during the final snow melting (March-April); the air temperature data are filtered with a low pass filter to enhance the diurnal variation of snow.
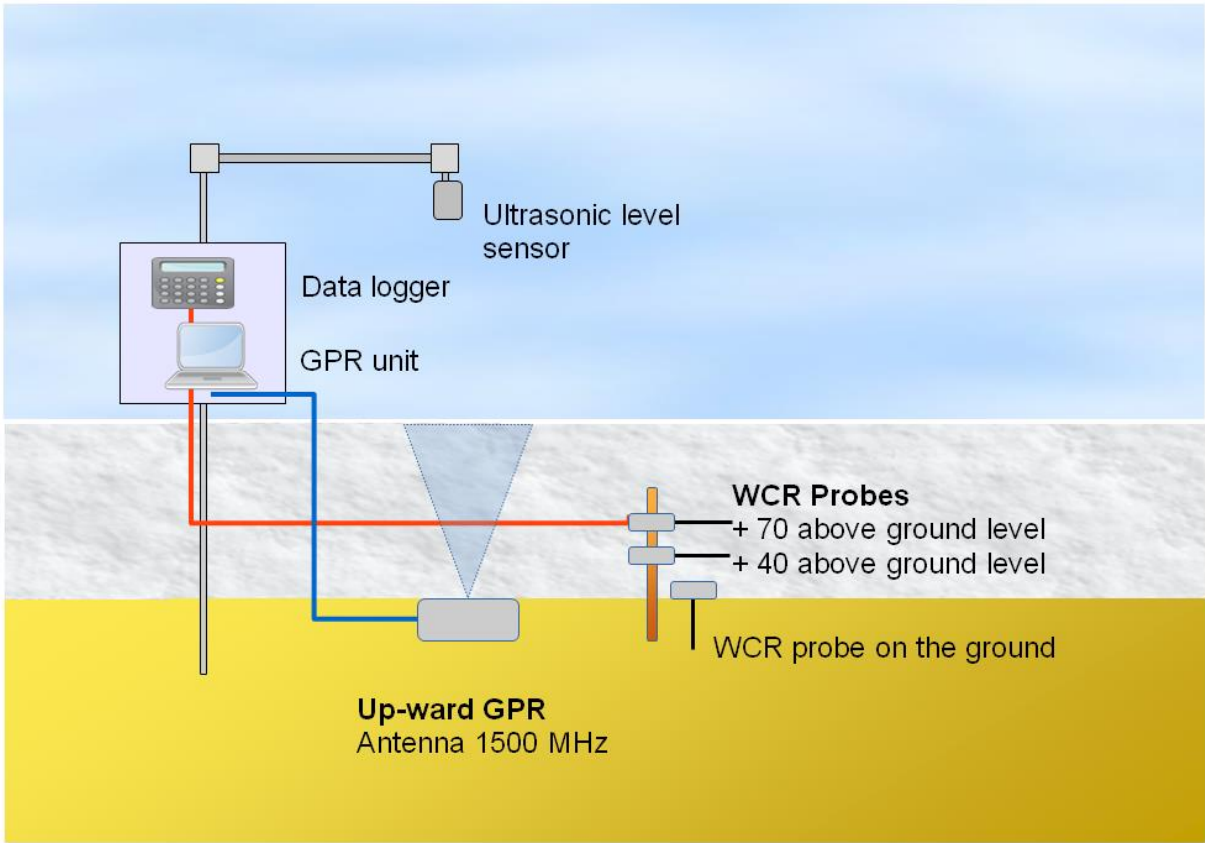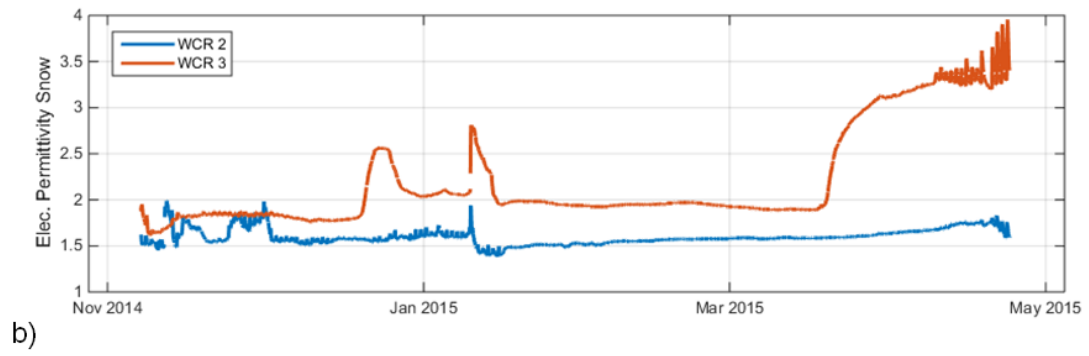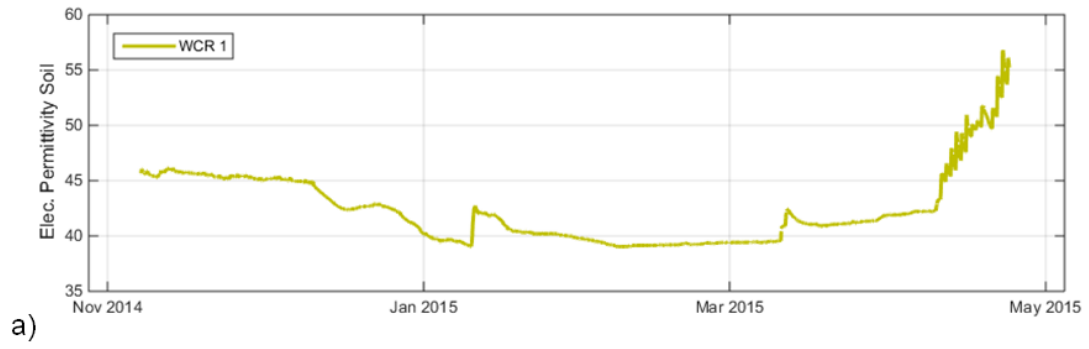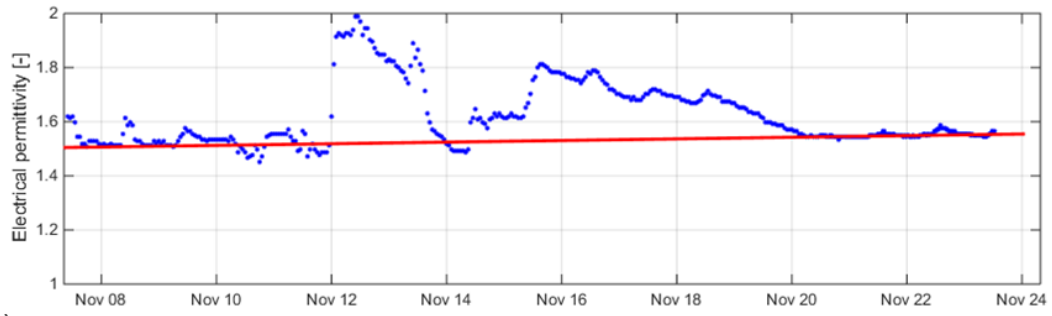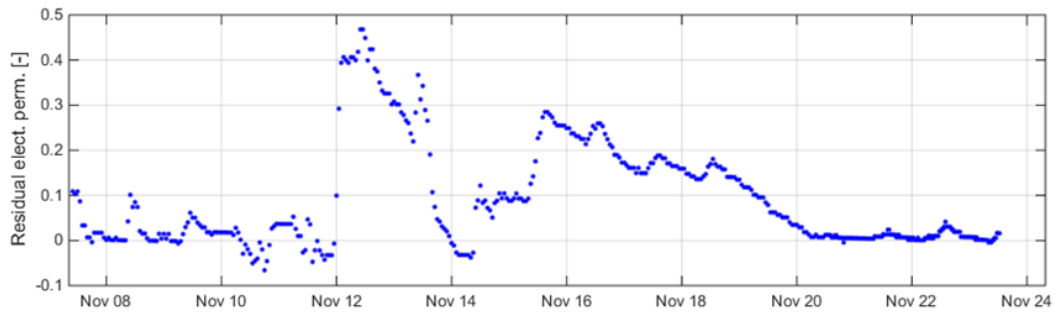
720
721   Figure 1
722

a)
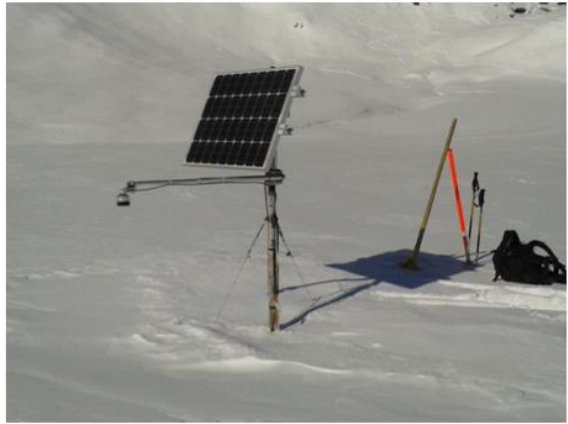
b)

723
724   Figure 2
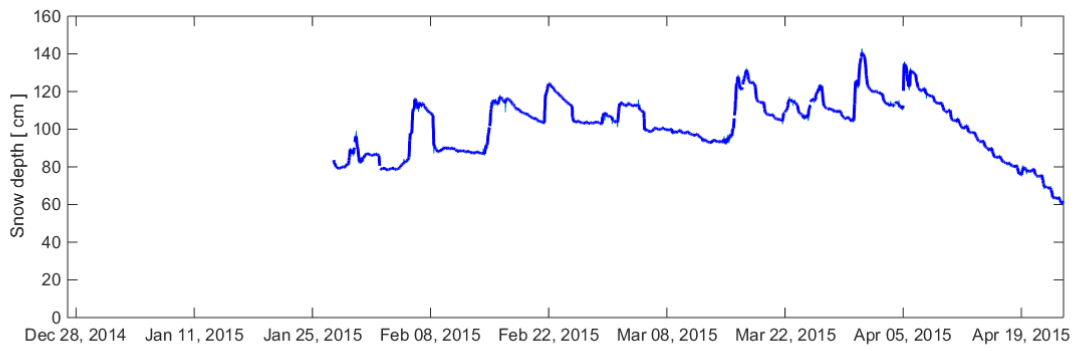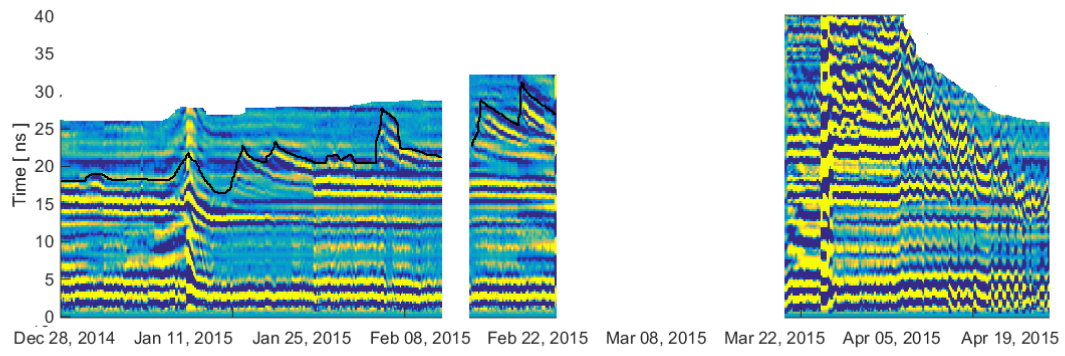725
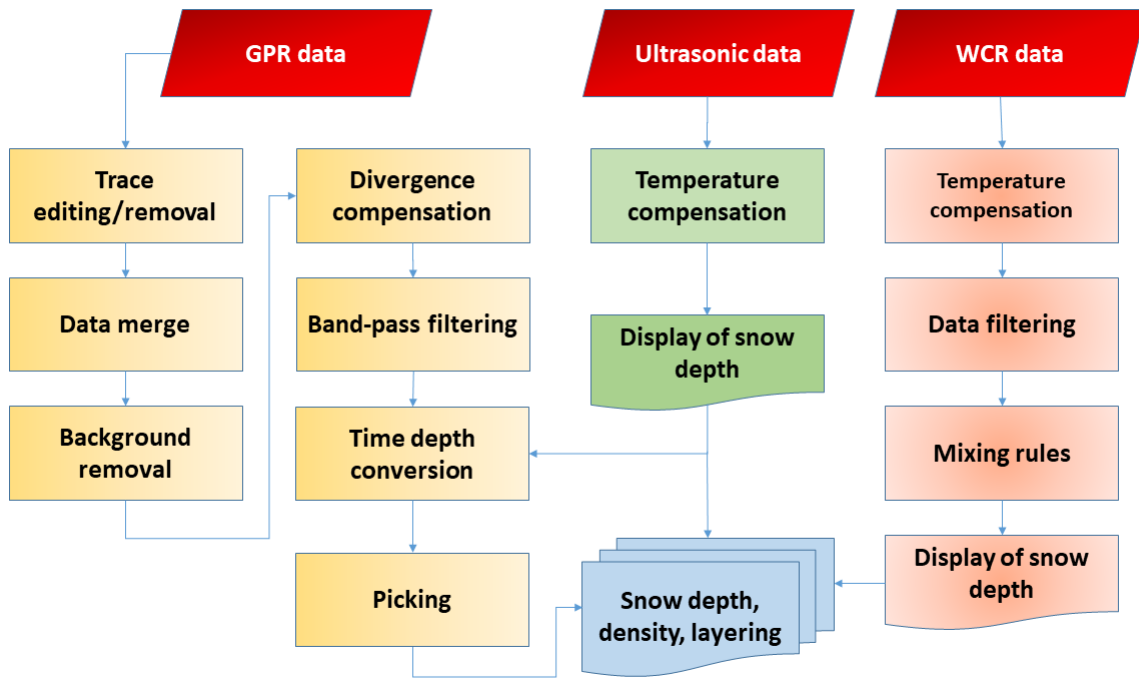
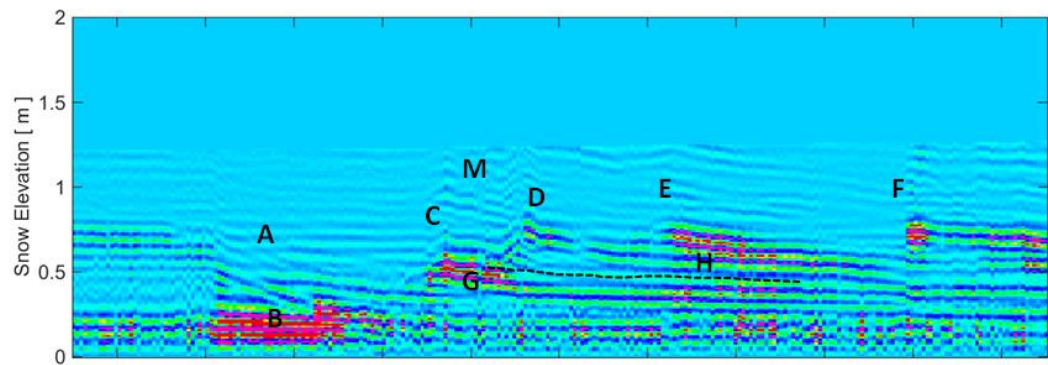726
727   Figure 3
728

a)

b)

729
730   Fugure 4
731

a)

b)
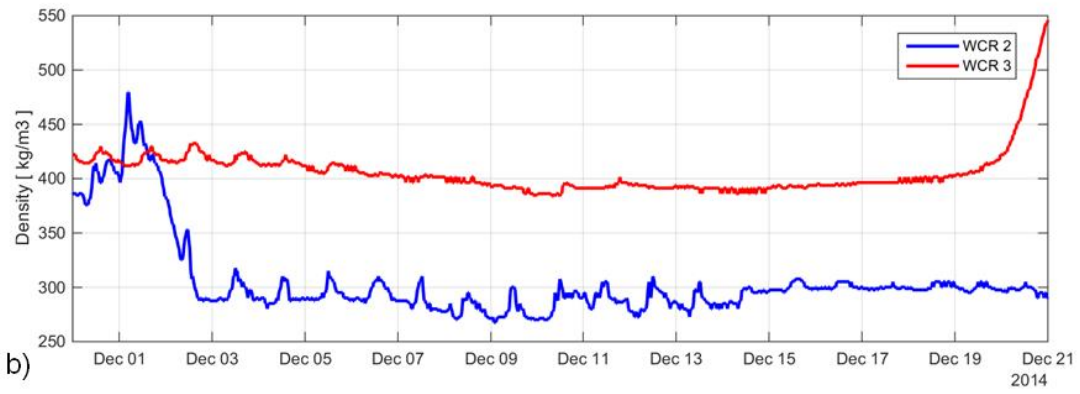
732
733   Figure 5
734

735
736   Figure 6
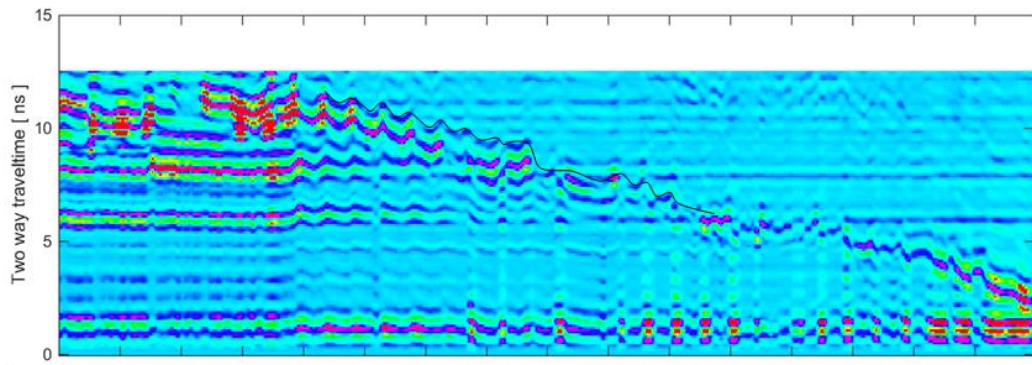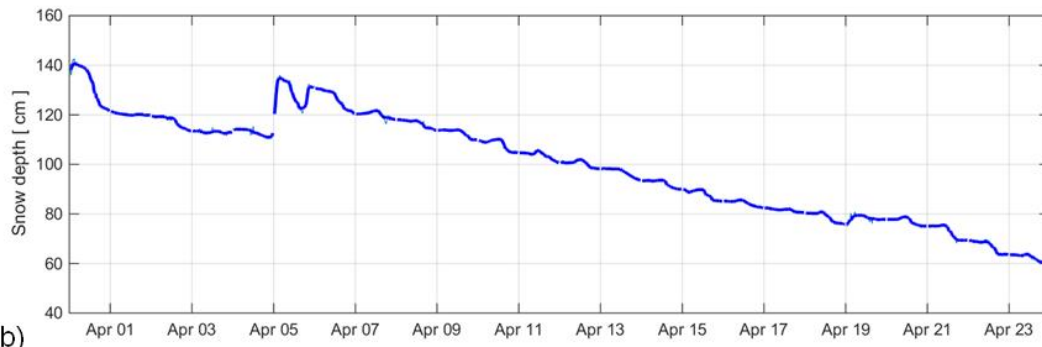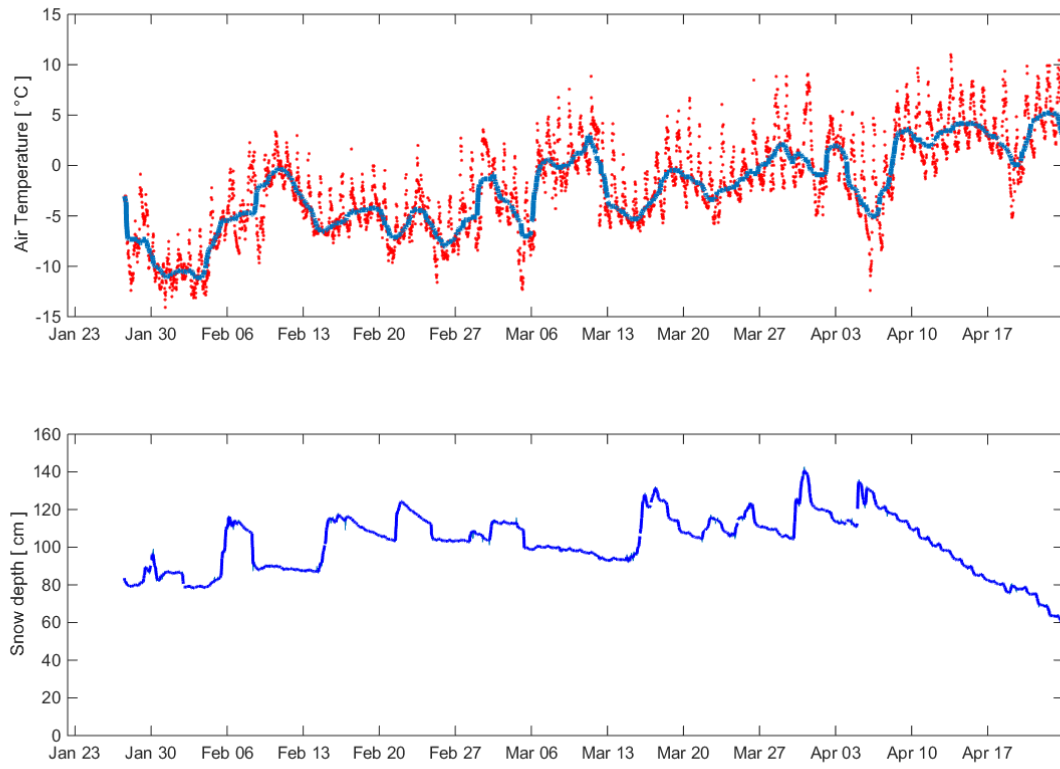737

738
739   Figure 7
740

741
742 Figure 8
743

744
745   Figure 9